Draft version January 21, 2022
Typeset using LaTeX **twocolumn** style in AASTeX631

Schwarzschild and Ledoux are equivalent on evolutionary timescales

Evan H. Anders,[1,2] Adam S. Jermyn,[3,2] Daniel Lecoanet,[1,4,2] Adrian E. Fraser,[5,2] Imogen G. Cresswell,[6,2] and J. R. Fuentes[7]

[1] *CIERA, Northwestern University, Evanston IL 60201, USA*
[2] *Kavli Institute for Theoretical Physics, University of California, Santa Barbara, CA 93106, USA*
[3] *Center for Computational Astrophysics, Flatiron Institute, New York, NY 10010, USA*
[4] *Department of Engineering Sciences and Applied Mathematics, Northwestern University, Evanston IL 60208, USA*
[5] *University of California, Santa Cruz, Santa Cruz, California 95064, U.S.A*
[6] *Department Astrophysical and Planetary Sciences & LASP, University of Colorado, Boulder, CO 80309, USA*
[7] *Department of Physics and McGill Space Institute, McGill University, 3600 rue University, Montreal, QC H3A 2T8, Canada*

(Received July 28, 2021; Revised October 19, 2021; Accepted; Published)

Submitted to ApJ

ABSTRACT

This will be an abstract.

Keywords: UAT keywords

1. INTRODUCTION

Observations tell us we don't understand the mixing at convective boundaries. For example, models and observations disagree about the sizes of convective cores (Claret & Torres 2018; Viani & Basu 2020; **?**), lithium abundances in solar-type stars (Pinsonneault 1997; Sestito & Randich 2005; Carlos et al. 2019; Dumont et al. 2021), and there is a well-known acoustic glitch in helioseismology at the base of the convection zone (see Basu 2016, Sec. 7.2.1). Improperly calculating the size of a convection zone can have important impacts across astrophysics such as setting the mass of stellar remnants (Farmer et al. 2019; Mehta et al. 2022) and affecting the inferred radii of exoplanets (Basu et al. 2012; Morrell 2020).

While there are many undercertainties in convective boundary mixing (CBM), the most fundamental question is: what sets the nominal boundary of the CZ? One way of answering this question is by evaluating the *Schwarzschild criterion*, which determines where the temperature and pressure stratification within a star are stable or unstable. The other answer is the *Ledoux criterion*, which accounts for stability or instability due to the composition (e.g., the variation of helium abundance with pressure; see Salaris & Cassisi 2017, chapter 3, for a nice review of these criteria). Recent work states that these criteria are logically equivalent at a convective boundary in the mixing length formalism (Gabriel et al. 2014; Paxton et al. 2018, 2019), but they are not always implemented to be that way (as in early versions of the MESA instrument, Paxton et al. 2013).

Modern studies still have not reached a consensus of which criterion to employ (see Kaiser et al. 2020, chapter 2, for a brief discussion). Multi-dimensional simulations have demonstrated that convection zones with Ledoux-stable boundaries expand by entraining compositionally-stable regions (Meakin & Arnett 2007; Woodward et al. 2015; Jones et al. 2017; Cristini et al. 2019; Fuentes & Cumming 2020; Andrassy et al. 2020, 2021). However, it is unclear from past 3D simulations whether that entrainment should stop at a Schwarzschild-stable boundary, leading to uncertainty in how to model entrainment in 1D models (Staritsin 2013; Scott et al. 2021).

In this work, we present a simple 3D hydrodynamical simulation that demonstrates that convection zones with Ledoux-stable but Schwarzschild-unstable boundaries will entrain material over roughly a thermal timescale until both the Ledoux and Schwarzschild criteria are equivalent at the convective boundary. Therefore, in 1D stellar evolution models, when the evolution time

Corresponding author: Evan H. Anders
evan.anders@northwestern.edu

is greater than or roughly equal to the thermal time (such as on the main sequence, see Georgy et al. 2021), these criteria should be implemented so that either one produces the same evolution. We briefly discuss these criteria in Sec. 2, display our simulations in Sec. **??**, and provide a brief discussion in Sec. 4.

2. THEORY

The stability of a convective region can instantaneously be determined using the Schwarzschild criterion,

$$\mathcal{Y}_{\rm S} = \nabla_{\rm rad} - \nabla_{\rm ad}, \tag{1}$$

or the Ledoux criterion,

$$\mathcal{Y}_{\rm L} = \nabla_{\rm rad} - \nabla_{\rm L}. \tag{2}$$

Here, $\mathcal{Y}$ is the discriminant (e.g., Paxton et al. 2018, sec. 2) or superadiabaticity. In stellar structure codes, it is assumed that regions with $\mathcal{Y} < 0$ are convection zones (CZs) while reagions with $\mathcal{Y} > 0$ are radiative zones (RZs).

When both stability criteria are considered, more interesting behavior can occur in certain physical regimes. A region is a CZ when both $\mathcal{Y}_{\rm S} < 0$ and $\mathcal{Y}_{\rm L} < 0$, and a region is an RZ when both $\mathcal{Y}_{\rm S} > 0$ and $\mathcal{Y}_{\rm L} \geq \mathcal{Y}_{\rm S}$. However, a "semiconvective" region is one that is Schwarzschild unstable ($\mathcal{Y}_{\rm S} < 0$) and Ledoux stable ($\mathcal{Y}_{\rm L} > 0$), and these regions can either be linearly stable or can exhibit overstable doubly-diffusive convection (ODDC, see Garaud 2018, chapter 2). CITES In this paper, we construct our initial conditions in our simulations so that the semiconvective regions are stable to ODDC, so that we can study the growth of convection zones through entrainment. Some RZs with $\mathcal{Y}_{\rm S} > \mathcal{Y}_{\rm L}$ (stable regions with unstable composition gradients) are also unstable to thermohaline or fingering convection (see Garaud 2018, chapter 3) CITE, but we do not study these regimes in this work.

In this work, we solve the simplest possible convective system. We utilize the Boussinesq approximation, which assumes that the depth of the layer being studied is much smaller than the local scale height. Since we are studying thin regions near convective boundaries, this assumption is OK. The relevant physics for this problem are included ($\nabla_{\rm rad}$ varies with height, buoyancy is determined both by the composition C and the temperature stratification T), so $\mathcal{Y}_{\rm S}$ and $\mathcal{Y}_{\rm L}$ are meaningfuly defined and distinct from one another when composition gradients are present. For details on our model setup and Dedalus simulations, we refer the reader to appendices A and B.

- The *instantaneous* stability changes over the course of many convective freefall times, and stellar evolution timesteps generally span many convective overturn times.
- The goal of this work is to find if y_S and y_L evolve toward the same value, and whether they evolve toward the initial boundary as determined by y_S or y_L.
- We will study a numerical simulation with three layers: a convective layer $y_s < 0$ and $y_L < 0$, a "semiconvective" (see section 4 of Paxton et al. 2013) (Salaris & Cassisi 2017) layer with $y_S < 0$ but $y_L > 0$ (which is stable to ODDC Garaud 2018), and a fully stable layer with $y_L > 0$ and $y_S > 0$.
- While "semiconvective" layers are often unstable to doubly-diffusive instabilities in stellar regimes (Moore & Garaud 2016), our purpose in this work is to demonstrate that regardless of whether these layers are doubly-diffusive unstable, they are entrained and destroyed by neighboring convective zones.

3. RESULTS

- We simulate a three-layer system with X properties using the Dedalus pseudospectral solver. We refer the reader to appendices A and B for details of the model assumptions, setup, and numerical methods.
- In figure **??** we show volume visualizations of instantaneous dynamics near the beginning, during the entrainment phase, and in the evolved state of one of these simulations. Here is a description of the things to look for in these visualizations. I should write this before I decide which things to put into this figure.
- In figure 1 we show horizontally- and time-averaged profiles of the initial state of the simulation, during the entrainment phase, and in the evolved state. Here's an in-depth description of what's plotted. Here's what you should take away from each panel of the plots.
- In figure 2, we plot a Kippenhahn-like diagram of the simulation. The orange region is the convection zone, the green region is Ledoux-stable but Schwarzschild-unstable, and the purple region is both Schwarzschild and Ledoux stable. The line at the top of the orange region determines the boundary of the convection zone according to y_L, and the line at the bottom of the purple region determines the CZ boundary according to y_S. While these

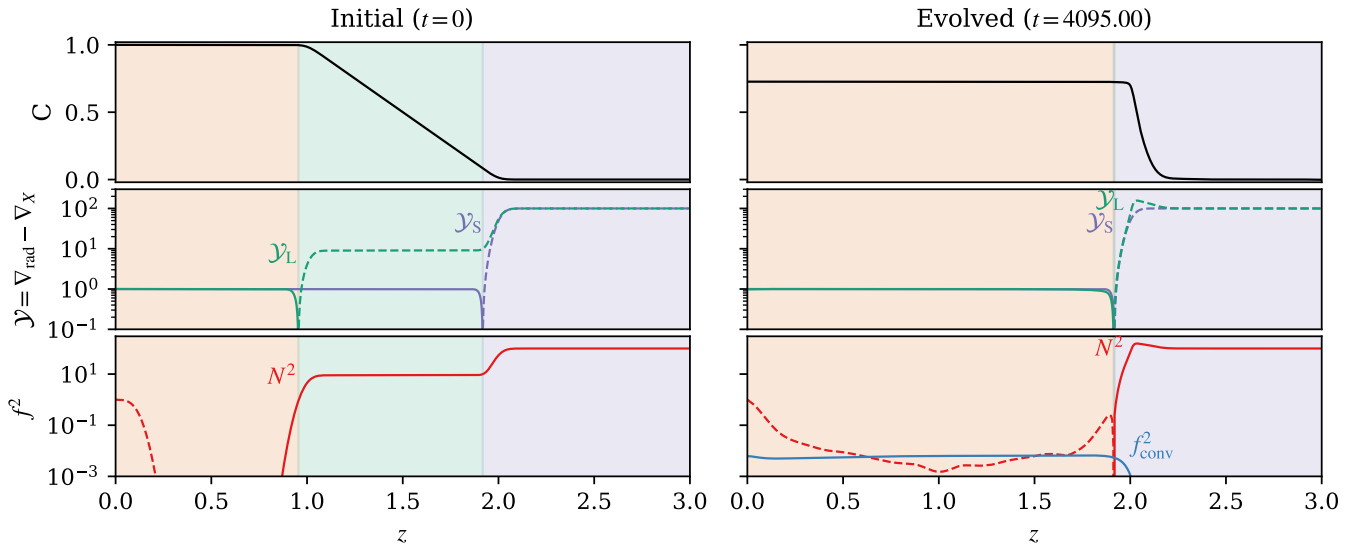

Figure 1.

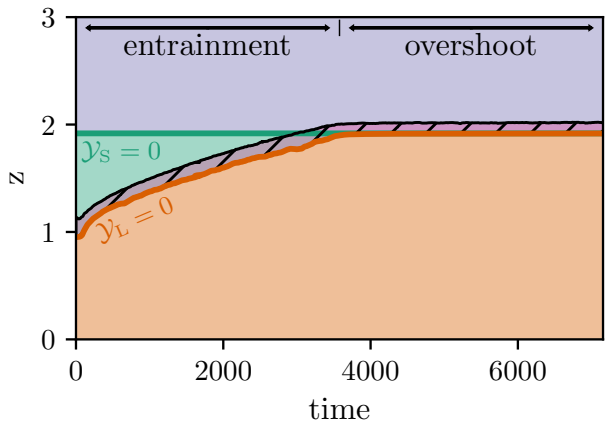

Figure 2.

lines start at different heights, convection entrains low-composition fluid according to a classic $\sqrt{t}$ entrainment law until these criteria are the same.

4. CONCLUSIONS

- We simulated X.
- These simulations demonstrate that the Schwarzschild criterion provides a good estimate of the boundary of the unstable convection zone.
- This analysis ignores secondary effects (e.g., convective penetration Anders et al. 2021, because we designed our experiments to minimize these effects).
- These results provide evidence from 3D dynamical simulations that modern implementations of MLT (Paxton et al. 2018, 2019) which are more logically consistent (Gabriel et al. 2014) are more accurate.
- Scott et al. (2021) simulates 1D main sequence models with entrainment at the core boundary. (cite staritsin 2013 too). They use an "entrainment law" similar to those found in 3D simulations, but find that thye need orders of magnitude lower entrainment to agree with observational constraints.
- Spruit (2015) gives some simple estimates of how entrainment rate can be calculated from buoyancy arguments.
- Our results demonstrate that while the Ledoux criterion is the proper *instantaneous* criterion for the boundary of convective regions, entrainment will erode stable composition gradients at convective boundaries. For stages in stellar evolution where $t_{\rm conv} \ll t_{\rm evolution}$, stellar evolution codes should use the Schwarzschild boundary; for stages where $t_{\rm conv} \lesssim t_{\rm evolution}$, future 3D numerical simulations should develop a more complete and parameterized theory of entrainment at convective boundaries, following the work of e.g., Turner (1968); Fuentes & Cumming (2020).
- Many Ledoux-stable but Schwarzschild-unstable regions in stars are unstable to ODDC (overstable doubly-diffusive convection), which has been theoretically described well in local models (Mirouh et al. 2012; Wood et al. 2013; Xie et al. 2017); these results are reviewed in Garaud (2018), applied to

main sequence stellar cores in Moore & Garaud (2016), and should be included in stellar models.

We thank Meridith Joyce, Anne Thoul, Dominic Bowman, ETC ETC ETC. EHA is funded as a CIERA Postdoctoral fellow and would like to thank CIERA and Northwestern University. This research was supported in part by the National Science Foundation under Grant No. PHY-1748958, and we acknowledge the hospitality of KITP during the Probes of Transport in Stars Program. Computations were conducted with support from the NASA High End Computing (HEC) Program through the NASA Advanced Supercomputing (NAS) Division at Ames Research Center on Pleiades with allocation GID s2276. The Flatiron Institute is supported by the Simons Foundation.

APPENDIX

A. MODEL & INITIAL CONDITIONS

In this work we study the simplest possible system: incompressible, Boussinesq convection with a composition field and a height-varying background radiative conductivity, similar to that used in Fuentes & Cumming (2020); Anders et al. (2021). These equations are

$$\boldsymbol{\nabla}\cdot\boldsymbol{u}=0, \tag{A1}$$

$$\partial_t\boldsymbol{u}\cdot\boldsymbol{\nabla}\boldsymbol{u}=-\frac{1}{\rho_0}\boldsymbol{\nabla}p+\frac{\rho_1}{\rho_0}\boldsymbol{g}+\nu\boldsymbol{\nabla}^2\boldsymbol{u}, \tag{A2}$$

$$\partial_t T+\boldsymbol{u}\cdot\boldsymbol{\nabla}T+w\nabla_{\rm ad}+\boldsymbol{\nabla}\cdot[-\kappa_{T,0}\boldsymbol{\nabla}\overline{T}]=\kappa_T\boldsymbol{\nabla}^2T', \tag{A3}$$

$$\partial_t C+\boldsymbol{u}\cdot\boldsymbol{\nabla}C=\kappa_{C,0}\boldsymbol{\nabla}^2\overline{C}+\kappa_C\boldsymbol{\nabla}^2C', \tag{A4}$$

$$\frac{\rho_1}{\rho_0}=-|\alpha|T+|\beta|C. \tag{A5}$$

Here, $\boldsymbol{u}$ is the vector velocity, T is the temperature, C is the composition, ρ_0 is the constant background density, p is the kinematic pressure which enforces Eqn. A1, ρ_1 are density fluctuations which act only on the buoyant term, and α and β are the thermal and compositional expansion coefficients, and $\nabla_{\rm ad}$ is the adiabatic gradient. Diffusive terms are controlled by the kinematic viscosity ν, as well as the thermal diffusivity κ_T and compositional diffusivity κ_C. On the horizontally-invariant ($n_x=0$ and $n_y=0$) mode, we use a height-depended thermal diffusion coefficient $\kappa_{T,0}$ (which allows $\nabla_{\rm rad}$ to vary with height) and a lower compositional diffusivity $\kappa_{C,0}<\kappa_C$ to ensure that the evolution of the mean composition profile is due to advection rather than diffusion.

We nondimensionalize Eqns. A1-A5 according to

$$\begin{aligned} &T^*=(\Delta T)T, \qquad C^*=(\Delta C)C, \qquad \partial_{t^*}=\tau_{\rm ff}^{-1}\partial_t, \qquad \boldsymbol{\nabla}^*=L_s^{-1}\boldsymbol{\nabla}, \qquad p^*=\rho_0 u_{\rm ff}^2\varpi,\\ &\boldsymbol{u}^*=u_{\rm ff}\boldsymbol{u}=\frac{L_s}{\tau_{\rm ff}}\boldsymbol{u}, \qquad \tau_{\rm ff}=\left(\frac{L_s}{|\alpha|g\Delta T}\right)^{1/2}, \qquad \kappa_{T,0}^*=(L_s^2\tau_{\rm ff}^{-1})\kappa_{T,0}. \end{aligned} \tag{A6}$$

For convenience, here we define quantities with $*$ (e.g., T^*) as being the "dimensionful" quantities of Eqns. A1-A5. Henceforth, quantities without $*$ (e.g., T) are dimensionless. Here, L_s is the length scale of the initial Schwarzschild-unstable convection zone and $\tau_f f$ is the buoyant freefall timescale. The temperature and composition are set by the destabilizing radiative temperature gradient $\Delta T=L_s(\partial_z T+\boldsymbol{\nabla}_{\rm ad})$ and the stabilizing composition gradient ($\Delta C=$

$L_s\partial_z C$). Within this nondimensionalization, the dynamical control parameters are

$$\mathcal{P} = \frac{u_{\rm ff} L_s}{\kappa_T}, \qquad \mathrm{R}_0 = \frac{|\alpha|\Delta T}{|\beta|\Delta C}, \qquad \mathrm{Pr} = \frac{\nu}{\kappa_T}, \qquad \tau = \frac{\kappa_C}{\kappa_T}, \qquad \tau_0 = \frac{\kappa_{C,0}}{\kappa_T} \tag{A7}$$

The dimensionless equations of motion are

$$\boldsymbol{\nabla}\cdot\boldsymbol{u} = 0 \tag{A8}$$

$$\partial_t \boldsymbol{u} + \boldsymbol{u}\cdot\boldsymbol{\nabla}\boldsymbol{u} = -\boldsymbol{\nabla}\varpi + (T - \mathrm{R}_0^{-1}C)\hat{z} + \frac{\mathrm{Pr}}{\mathcal{P}}\boldsymbol{\nabla}^2\boldsymbol{u} \tag{A9}$$

$$\partial_t T + \boldsymbol{u}\cdot\boldsymbol{\nabla}T + w\boldsymbol{\nabla}_{\rm ad} + \boldsymbol{\nabla}\cdot[-\kappa_{T,0}\boldsymbol{\nabla}\overline{T}] = \frac{1}{\mathcal{P}}\boldsymbol{\nabla}^2 T'., \tag{A10}$$

$$\partial_t C + \boldsymbol{u}\cdot\boldsymbol{\nabla}C = -\frac{\tau_0}{\mathcal{P}}\boldsymbol{\nabla}^2\overline{C} + \frac{\tau}{\mathcal{P}}\boldsymbol{\nabla}^2 C'. \tag{A11}$$

We define the thermal and compositional gradients

$$\nabla_{\rm T} \equiv -\frac{\partial T}{\partial z}, \qquad \nabla_{\rm C} \equiv -\mathrm{R}_0^{-1}\frac{\partial C}{\partial z}, \tag{A12}$$

and stability is determined by the sign of the Brunt-Väisälä frequency,

$$N^2 = N^2_{\rm structure} + N^2_{\rm composition}, \text{ with } N^2_{\rm structure} = -(\nabla_{\rm T} - \nabla_{\rm ad}),\ N^2_{\rm composition} = \nabla_{\rm C}, \tag{A13}$$

where $N^2 > 0$ is buoyantly stable, so the stability criterion is $\nabla_{\rm C} - (\nabla_{\rm T} - \nabla_{\rm ad}) > 0$, as in stellar models (Salaris & Cassisi 2017).

In this work, we study a three-layer model in $z = [0, 3]$. We want to construct a simulation with

$$N^2 = \begin{cases} -1 & z \le 1 \\ R_0^{-1} - 1 & 1 < z \le 2\,, \\ R_0^{-1} & 2 < z \end{cases} \qquad N^2_{\rm composition} = \begin{cases} 0 & z \le 1 \\ R_0^{-1} & 1 < z \le 2\,, \\ 0 & 2 < z \end{cases} \qquad N^2_{\rm structure} = \begin{cases} -1 & z \le 1 \\ -1 & 1 < z \le 2 \\ R_0^{-1} & 2 < z \end{cases} \tag{A14}$$

To achieve this, we set $\partial_z C = -\mathrm{R}_0 N^2_{\rm composition}$ and $\partial_z T = N^2_{\rm structure} - \nabla_{\rm ad}$, where we set $\nabla_{\rm ad} = 5[\mathrm{R}_0^{-1} - 2]$ as a constant so that $\nabla_{\rm ad} > 0$ for all values of R_0 studied. We furthermore enforce that $\nabla_{\rm T} = \nabla_{\rm rad}$ in the initial state, where

$$\nabla_{\rm rad} = -\frac{F_{\rm tot}}{\kappa_{T,0}}, \tag{A15}$$

is the radiative gradient and $F_{\rm tot}$ is the total vertical energy flux through the system. We set the total flux $F_{\rm tot} = -(1 + \nabla_{\rm ad})/\mathcal{P}$ and the convective flux $F_{\rm conv} = 1/\mathcal{P}$, so $\kappa_{T,0}(z) = -((1 + \nabla_{\rm ad})/\partial_z T)\mathcal{P}^{-1}$.

B. SIMULATION DETAILS & DATA AVAILABILITY

We time-evolve equations ?? using the Dedalus pseudospectral solver (Burns et al. 2020) using timestepper SBDF2 (Wang & Ruuth 2008) and safety factor 0.3. All fields are represented as spectral expansions of n_z Chebyshev coefficients in the vertical (z) direction and as (n_x, n_y) Fourier coefficients in the horizontal (x, y) directions; our domain is therefore horizontally periodic. We use a domain with an aspect ratio of two so that $x \in [0, L_x]$, $y \in [0, L_y]$, and $z \in [0, L_z]$ with $L_x = L_y = 2L_z$. The initial convection zone spans initially spans 1/3 of the domain depth and in the evolved state spans 2/3 of the domain depth, so it has an initial aspect ratio of 6 and a final aspect ratio of 3. To avoid aliasing errors, we use the 3/2-dealiasing rule in all directions. To start our simulations, we add random noise temperature perturbations with a magnitude of 10^{-6} to the initial temperature profile (discussed in ??).

Spectral methods with finite coefficient expansions cannot capture true discontinuities. In order to approximate discontinuous functions such as Eqns. A14, we must use smooth transitions. We therefore define a smooth Heaviside step function,

$$H(z; z_0, d_w) = \frac{1}{2}\left(1 + \mathrm{erf}\left[\frac{z - z_0}{d_w}\right]\right). \tag{B16}$$

where erf is the error function. In the limit that $d_w \to 0$, this function behaves identically to the classical Heaviside function centered at z_0. Throughout this work, we set $d_w = 0.05$.

A table describing all of the simulations presented in this work can be found in Appendix C. We produce figures ?? and ?? using matplotlib (Hunter 2007; Caswell et al. 2021). We produce figure ?? using TODO. All of the Python scripts used to run the simulations in this paper and to create the figures in this paper are publicly available in a git repository[1], and in a Zenodo repository (**?**).

C. TABLE OF SIMULATION PARAMETERS

Input parameters and summary statistics of the simulations presented in this work are shown in Table **??**.

REFERENCES

Anders, E. H., Jermyn, A. S., Lecoanet, D., & Brown, B. P. 2021, arXiv e-prints, arXiv:2110.11356. https://arxiv.org/abs/2110.11356

Andrassy, R., Herwig, F., Woodward, P., & Ritter, C. 2020, MNRAS, 491, 972, doi: 10.1093/mnras/stz2952

Andrassy, R., Higl, J., Mao, H., et al. 2021, arXiv e-prints, arXiv:2111.01165. https://arxiv.org/abs/2111.01165

Basu, S. 2016, Living Reviews in Solar Physics, 13, 2, doi: 10.1007/s41116-016-0003-4

Basu, S., Verner, G. A., Chaplin, W. J., & Elsworth, Y. 2012, ApJ, 746, 76, doi: 10.1088/0004-637X/746/1/76

Burns, K. J., Vasil, G. M., Oishi, J. S., Lecoanet, D., & Brown, B. P. 2020, Physical Review Research, 2, 023068, doi: 10.1103/PhysRevResearch.2.023068

Carlos, M., Meléndez, J., Spina, L., et al. 2019, MNRAS, 485, 4052, doi: 10.1093/mnras/stz681

Caswell, T. A., Droettboom, M., Lee, A., et al. 2021, matplotlib/matplotlib: REL: v3.3.4, v3.3.4, Zenodo, doi: 10.5281/zenodo.4475376

Claret, A., & Torres, G. 2018, ApJ, 859, 100, doi: 10.3847/1538-4357/aabd35

Cristini, A., Hirschi, R., Meakin, C., et al. 2019, MNRAS, 484, 4645, doi: 10.1093/mnras/stz312

Dumont, T., Palacios, A., Charbonnel, C., et al. 2021, A&A, 646, A48, doi: 10.1051/0004-6361/202039515

Farmer, R., Renzo, M., de Mink, S. E., Marchant, P., & Justham, S. 2019, ApJ, 887, 53, doi: 10.3847/1538-4357/ab518b

Fuentes, J. R., & Cumming, A. 2020, Physical Review Fluids, 5, 124501, doi: 10.1103/PhysRevFluids.5.124501

Gabriel, M., Noels, A., Montalbán, J., & Miglio, A. 2014, A&A, 569, A63, doi: 10.1051/0004-6361/201423442

Garaud, P. 2018, Annual Review of Fluid Mechanics, 50, 275, doi: 10.1146/annurev-fluid-122316-045234

Georgy, C., Saio, H., & Meynet, G. 2021, A&A, 650, A128, doi: 10.1051/0004-6361/202040105

Hunter, J. D. 2007, Computing in Science and Engineering, 9, 90, doi: 10.1109/MCSE.2007.55

Jones, S., Andrassy, R., Sandalski, S., et al. 2017, MNRAS, 465, 2991, doi: 10.1093/mnras/stw2783

Kaiser, E. A., Hirschi, R., Arnett, W. D., et al. 2020, MNRAS, 496, 1967, doi: 10.1093/mnras/staa1595

Meakin, C. A., & Arnett, D. 2007, ApJ, 667, 448, doi: 10.1086/520318

Mehta, A. K., Buonanno, A., Gair, J., et al. 2022, ApJ, 924, 39, doi: 10.3847/1538-4357/ac3130

Mirouh, G. M., Garaud, P., Stellmach, S., Traxler, A. L., & Wood, T. S. 2012, ApJ, 750, 61, doi: 10.1088/0004-637X/750/1/61

Moore, K., & Garaud, P. 2016, ApJ, 817, 54, doi: 10.3847/0004-637X/817/1/54

Morrell, S. A. F. 2020, PhD thesis, University of Exeter

Paxton, B., Cantiello, M., Arras, P., et al. 2013, ApJS, 208, 4, doi: 10.1088/0067-0049/208/1/4

Paxton, B., Schwab, J., Bauer, E. B., et al. 2018, ApJS, 234, 34, doi: 10.3847/1538-4365/aaa5a8

Paxton, B., Smolec, R., Schwab, J., et al. 2019, ApJS, 243, 10, doi: 10.3847/1538-4365/ab2241

Pinsonneault, M. 1997, ARA&A, 35, 557, doi: 10.1146/annurev.astro.35.1.557

Salaris, M., & Cassisi, S. 2017, Royal Society Open Science, 4, 170192, doi: 10.1098/rsos.170192

Scott, L. J. A., Hirschi, R., Georgy, C., et al. 2021, MNRAS, 503, 4208, doi: 10.1093/mnras/stab752

Sestito, P., & Randich, S. 2005, A&A, 442, 615, doi: 10.1051/0004-6361:20053482

Spruit, H. C. 2015, A&A, 582, L2, doi: 10.1051/0004-6361/201527171

Staritsin, E. I. 2013, Astronomy Reports, 57, 380, doi: 10.1134/S1063772913050089

Turner, J. S. 1968, Journal of Fluid Mechanics, 33, 183, doi: 10.1017/S0022112068002442

[1] https://github.com/evanhanders/convective_penetration_paper

Viani, L. S., & Basu, S. 2020, ApJ, 904, 22, doi: 10.3847/1538-4357/abba17

Wang, D., & Ruuth, S. J. 2008, Journal of Computational Mathematics, 26, 838. http://www.jstor.org/stable/43693484

Wood, T. S., Garaud, P., & Stellmach, S. 2013, ApJ, 768, 157, doi: 10.1088/0004-637X/768/2/157

Woodward, P. R., Herwig, F., & Lin, P.-H. 2015, ApJ, 798, 49, doi: 10.1088/0004-637X/798/1/49

Xie, J.-H., Miquel, B., Julien, K., & Knobloch, E. 2017, Fluids, 2, doi: 10.3390/fluids2010006